Accuracy of the pneumatic method for estimating xylem vulnerability to embolism in temperate diffuse-porous tree species

Sharath S. Paligi[1,2,*], Roman M. Link[1,7,*], Emilie Isasa[1], Paulo Bittencourt[3], Juliano Sarmento Cabral[4], Steven Jansen[5], Rafael S. Oliveira[6], Luciano Pereira[5], Bernhard Schuldt[1,7]

[1] *University of Würzburg, Julius-von-Sachs-Institute of Biological Sciences, Chair of Ecophysiology and Vegetation Ecology, Julius-von-Sachs-Platz 3, 97082 Würzburg, Germany*

[2] Present address: *Plant Ecology and Ecosystems Research, Albrecht von Haller Institute for Plant Sciences, University of Göttingen, Göttingen, Germany*

[3] *College of Life and Environmental Sciences, University of Exeter, Exeter, United Kingdom*

[4] *Ecosystem Modeling Group, Center for Computational and Theoretical Biology, University of Würzburg, Würzburg, Germany*

[5] *Institute of Systematic Botany and Ecology, Albert-Einstein-Allee 11, Ulm University, D-89081 Ulm, Germany*

[6] *Department of Plant Biology, Instituto de Biologia, University of Campinas, Caixa Postal 6109, CEP 13083-970, Campinas, SP, Brazil*

[7] *Corresponding authors:* roman.link@plant-ecology.de
bernhard.schuldt@plant-ecology.de

[*] First and second author contributed equally to this work

Running title: Accuracy of the pneumatic method

Word count:	Summary	200
	Main body	6,316
	Introduction	1,040
	Materials and methods	2,232
	Results	695
	Discussion	2,363
	Acknowledgements	68
	Tables	2
	Figures	5
	Supporting information	6

Keywords: Cavitron, drought tolerance traits, xylem embolism resistance, vulnerability curve, methods comparison, Pneumatron, plant hydraulics.

Summary

- The increasing frequency of global change-type droughts has created a need for fast, accurate and widely applicable techniques for estimating xylem embolism resistance to improve forecasts of future forest changes.

- We used data from 12 diffuse-porous temperate tree species covering a wide range of xylem safety to compare the pneumatic and flow-centrifuge method for constructing xylem vulnerability curves. We evaluated the agreement between parameters estimated with both methods and the sensitivity of pneumatic measurements to the measurement duration.

- The agreement between xylem water potentials at 50% air discharged (PAD) estimated with the Pneumatron and 50% loss of hydraulic conductivity (PLC) estimated with the flow-centrifuge method was high (mean signed deviation: 0.12 MPa, Pearson correlation: 0.96 after 15 sec of gas extraction). However, the relation between the estimated slopes was more variable, resulting in lower agreement in xylem water potential at 12% and 88% PAD/PLC. All parameters were sensitive to the duration of the pneumatic measurement, with highest overall agreement between methods after 16 sec.

- We conclude that, if applied correctly, the pneumatic method enables fast and inexpensive estimations of embolism resistance for a wide range of temperate, diffuse-porous species, which makes it attractive for predicting plant performance under climate change.

Introduction

In the last decades, unprecedented climate fluctuations and the resulting extreme drought events have led to large-scale tree dieback events worldwide (Allen *et al*., 2010, 2015; Brando *et al*., 2019). With the global rise in frequency, intensity and duration of drought spells predicted by current climate projections (cf. Field *et al*., 2012; Trenberth *et al*., 2014), large-scale drought-induced tree mortality events become increasingly likely (Brodribb *et al*., 2020).

To improve the prediction of demographic and compositional changes in forest ecosystems, a better understanding of physiological mechanisms associated with the death of trees in response to drought is necessary (Allen *et al*., 2010; McDowell *et al*., 2013a, 2013b). In this context, traits that quantify the vulnerability of a tree's xylem to drought-induced embolism have received particular attention (Choat *et al*., 2018; Brodribb *et al*., 2020). Vulnerability to embolism is usually expressed by the parameters of xylem vulnerability curves (VCs), i.e. curves describing the consecutive loss of hydraulic conductance (percent loss of conductivity, PLC) as a function of increasingly negative xylem pressures (cf. Sperry *et al*., 1988; Cochard *et al*., 2013). Most commonly, VCs are described by the water potential at 12, 50 or 88% loss of hydraulic conductance (P_{12}, P_{50} and P_{88}, respectively) and the slope of the curve at one of the respective locations. The parameters of VCs have been linked to mechanistic thresholds for xylem functioning (cf. Brodribb & Cochard, 2009; Urli *et al*., 2013; Delzon & Cochard, 2014), and are closely coordinated with stomatal regulation (Martin-StPaul *et al*., 2017). Across biomes, xylem embolism resistance has been associated with the susceptibility of a species to drought-induced mortality (Anderegg *et al*., 2016; Adams *et al*., 2017; Correia *et al*., 2019; Powers *et al*., 2020) and thus mirrors the distribution of species along aridity gradients (Blackman *et al*., 2014; Trueba *et al*., 2017; Oliveira *et al*., 2019). Due to their immediate mechanistic interpretation, VC parameters and derived quantities such as hydraulic safety margins (Meinzer *et al*., 2009) are increasingly incorporated in process-based vegetation models to describe plant drought responses and associated drought-induced tree mortality

(McDowell *et al*., 2013a, 2013b; Christoffersen *et al*., 2016; Xu *et al*., 2016; Davi & Cailleret 2017; Eller *et al*., 2020).

Xylem VCs can be established through a large number of different techniques, such as the bench dehydration (Sperry *et al*., 1988), air injection (Cochard *et al*., 1992), flow-centrifuge (Cochard *et al*., 2005), micro-CT (Brodersen *et al*., 2010), pneumatic (Pereira *et al*., 2016), optical (Brodribb *et al*., 2016) and relative water loss method (Rosner *et al*., 2019). However, none of these methods is unequivocally reliable for angiosperm and gymnosperm species, either due to measurement artefacts associated with vessel length and porosity (Cochard *et al*., 2013; Jansen *et al*., 2015) or because they are not suitable for rapid measurements of large number of samples (Cochard *et al*., 2013; Nolf *et al*., 2017). Given their usefulness to predictive models, methods for the measurement of xylem embolism that are simple, accessible, reliable and applicable for a wide range of taxonomic groups and xylem types are needed.

A novel, promising route for fast indirect VC measurements is the pneumatic method (Pereira *et al*., 2016; Jansen *et al*., 2020), which estimates the amount of xylem embolism by measuring the increase of air volume in the xylem in bench-dried plant samples with increasingly negative xylem pressure. Recently, Pereira *et al*. (2020) proposed an automated device, the Pneumatron, which automatically measures air discharge from a plant sample at a high temporal resolution and permits a high sample throughput. As the measurement principle of the Pneumatron does not directly depend on the measurement of xylem water transport, and embolism is induced by bench dehydration, it is assumed to be relatively robust against measurement artefacts related to sample excision and preparation as well as vessel length related artefacts (Pereira *et al*., 2016, 2020), which are known to affect several hydraulic VC methods (cf. Choat *et al*., 2010; Wheeler *et al*., 2013; Martin-StPaul *et al*., 2014; Torres-Ruiz *et al*., 2014, 2015).

The pneumatic method has already been applied to construct VCs for branches, leaves and roots of tropical, subtropical and temperate species, covering diffuse-porous, ring-porous and coniferous species (Pereira *et al*., 2016, 2020; Zhang *et al*., 2018; Wu *et al*., 2020; Sergent *et*

al., 2020). The results from these studies indicate the suitability of the method for diffuse-porous (Pereira *et al*., 2016; Zhang *et al*., 2018; Sergent *et al*., 2020) and for ring-porous species (though the latter only after gluing growth rings other than the current year rings; cf. Zhang *et al*., 2018). However, Zhang *et al*. (2018) reported that the pneumatic method resulted in lower estimates of embolism resistance of two conifer species compared to the flow-centrifuge method. Similarly, in a recent methodological comparison of VC techniques, Sergent *et al*. (2020) found the pneumatic method to result in lower embolism resistance estimates compared to other methods in further two conifer species, and reported inconsistent estimates for long-vesseled species. Several sources of uncertainty have been identified for the pneumatic method that leave room for potential methodological improvements. Notably, its estimates are known to be sensitive to the choice of the reservoir volume and the duration of the air discharge measurement (Pereira *et al*., 2016, 2020). Prior studies have used vastly different time intervals to measure air discharge (AD) from the xylem segment, ranging from 150 sec (Pereira *et al*., 2016; Chen *et al*., 2021), over 120 sec (Zhang *et al*., 2018; Sergent *et al*., 2020; Wu *et al*., 2020), to only 30 sec (Pereira *et al*., 2020). Since a 15 sec duration was predicted as optimal discharge time based on the Unit Pipe Pneumatic model (Yang *et al*., 2021), there is a need to test this hypothesis experimentally. Moreover, despite considerable attention to measuring artefacts and methodological concerns, we currently lack a rigorous statistical framework to compare embolism resistance methods.

This study uses a dataset of vulnerability curve measurements from 36 trees belonging to 12 temperate, diffuse-porous tree species to i) assess how well the parameters of the vulnerability curves obtained with the pneumatic method (Pneumatron) agree with estimates obtained from the flow-centrifuge method (Cavitron) in terms of systematic deviations, random deviations and overall agreement, and to ii) identify the optimal duration for air discharge measurements.

Materials and Methods

Plant material

Plant material from trees belonging to 12 temperate diffuse-porous tree species (Table 1) was collected between mid-July and mid-September 2019 from a nursery in Veitshöchheim (49°50'24.3"N, 9°52'38.4"E) near Würzburg, Germany. These trees were planted in the year 2011 in the framework of a long-term comparative experiment designed to identify appropriate tree species for urban planting. The plant material cultivated in Veitshöchheim was obtained from selected nurseries across Central Europe. Due to anomalies in the data for some of the species (see below), additional branch samples were obtained from adult *Tilia cordata* and *Tilia platyphyllos* trees growing at Ulm University, Germany (48°25'20.3"N, 9°57'20.2"E) and of *Tilia japonica* from the Würzburg botanical garden (49°45'56.7"N 9°55'58.1"E) in September 2020.

The samples were collected before 9:30 a.m. to assure sample excision took place in a relaxed state, thus avoiding measurement artefacts associated with cutting under tension (Wheeler *et al*., 2013). From each of the experimental trees, one sun-exposed branch 70 - 120 cm in length or any kind of damage to avoid leaks and consequent embolism overestimation. All suspicious leakage points were sealed using a fast-drying contact adhesive (Loctite 431 with Loctite activator SF 7452, Henkel, Düsseldorf, Germany). Fruits present on the branches were removed and sealed with the same glue, as they easily detach with progressing dehydration and are hence a potential site of air-entry. Similarly, in the case of *Crataegus persimilis*, thorns were removed and sealed in the same manner to ease the handling of the branches.

Measurements of vulnerability curves with the pneumatic method

Branch xylem vulnerability curves based on the pneumatic method (Pereira *et al*., 2016) were obtained for 44 samples from 35 experimental trees (Table 1) using the Pneumatron, a device

that combines a microcontroller-activated vacuum pump and a pressure transducer to allow for automated measurements of air discharge (Pereira *et al*., 2020; Jansen *et al*., 2020).

The reservoir pressure was tracked with the Pneumatron in 0.5 sec intervals over a span of two minutes per measurement (including a pump time of approximately 2 sec in semi-automated mode and few milliseconds in automated mode). The amount of air discharged (AD) into the reservoir was calculated based on the ideal gas law (Pereira *et al*., 2016). The semi-automated mode of the Pneumatron was used to measure AD for the samples obtained from Veitshöchheim and Würzburg, whereas the additional branch samples of *T. cordata* and *T. platyphyllos* processed in Ulm were measured in automated mode. After each AD measurement, the xylem water potential was measured (see below). The maximum detectable amount of AD is associated with a change of pressure in the system by ~50 kPa (Pereira *et al*., 2020). As the time necessary for a pressure change of 50 kPa depends on the ratio between the reservoir volume (including the cut-open conduit volume) and the volume of gas extracted from intact, embolised conduits, the choice of the optimal reservoir volume is crucial (cf. Pereira *et al*., 2020). For this study, reservoir volumes of 1.7 – 3.3 ml were selected based on the available information about the species' embolism resistance from the xylem functional traits database (Choat *et al*., 2012), assuming that higher embolism resistance corresponds to a lower volume of gas extracted from intact, embolised conduits and hence a lower optimal reservoir volume and vice-versa. Meanwhile, however, Pereira *et al*. (2020), recommend determining the maximum reservoir volume from a completely dried branch per species. Throughout the measurements, the volume of the vacuum reservoir was kept constant for each branch.

Once the branch was fully hydrated, a clean cut was made in air at the basipetal end using a sharp razor blade to clear obstructions for air flow (Pereira *et al*., 2016; Jansen *et al*., 2020). Although this seems counterintuitive at first glance, cutting in air was done intentionally because the cut-open conduits need to be embolised when starting pneumatic measurements. The branch was then connected to the pneumatic apparatus using rigid and elastic tubing, plastic

147 clamps and three-way stopcocks (Fig. S1, S2). The volume of the elastic tube was kept as small
148 as possible to minimize pressure-dependent changes in reservoir volume. The elastic tubing
149 was tightened with a plastic clamp to ensure no leakage occurred during the measurement
150 (Bittencourt *et al*., 2018). Before each series of measurements and in case of suspicious
151 increases in the amount of AD, the connections and the plant material were thoroughly
152 inspected to identify and seal potential air-entry points.
153 Before AD measurements were taken, the branch samples were bagged in dark plastic bags to
154 equilibrate water potential. During AD measurement, the branches were kept bagged to
155 minimize transpiration. Between measurements, the branches were dehydrated at room
156 temperature on a laboratory bench to induce embolism (Sperry *et al*., 1988). The branches were
157 initially dried for intervals of about 15 – 30 min, which were subsequently increased to 1 – 4 h
158 depending on how quickly the sample dried. To allow xylem water potential to equilibrate after
159 each drying interval, the samples were bagged for about 30 min in the initial steps of
160 dehydration, and for at least one hour in the later stages to account for the decrease in the leaf-
161 stem conductance (cf. Pereira *et al*., 2016). AD measurements were made on multiple branches
162 on the same day (see Fig. S1 – S3). The elastic tubing was always kept connected to the branch
163 samples when switching branches to keep the reservoir volume constant throughout all
164 measurements. AD measurements were taken until the branches were completely dehydrated
165 and no considerable variation was observed in the amount of AD in consecutive measurements
166 over at least 24 h, or until the maximum absolute xylem water potential measurable with the
167 Scholander pressure chamber (10 MPa) was reached. This resulted in measurement durations
168 of 3 – 7 days as well as in 10 – 20 AD and leaf water potential measurements per branch when
169 following the semi-automated mode of the Pneumatron. The percentage of air discharged
170 (PAD) was calculated as described by Pereira *et al*. (2016):

171 $$PAD_i = 100 * (AD_i - AD_{min}) / (AD_{max} - AD_{min}), \quad (1)$$

where AD_i is the amount of air discharged for measurement *i*, AD_{min} is the minimum amount of air discharged from the fully hydrated branch, and AD_{max} is the maximum amount of air discharged from the branch when completely desiccated.

Xylem water potential measurement

For the 35 branch samples measured in semi-automated mode, the xylem pressure was measured with a Scholander pressure chamber (PMS Instruments, Corvallis, Oregon, USA) after every AD measurement. At each pressure step, two leaves were cut-off from the branch, and xylem water potential was averaged over two pressure chamber measurements. When the petiole was too small for measurement in the pressure chamber, small terminal twigs were used. The cut was immediately sealed using an instant adhesive (Loctite 431) to prevent leakage during the subsequent AD measurements. For the nine branches of *T. cordata* and *T. platyphyllos* measured using the automated mode of a Pneumatron, a stem psychrometer (ICT International, Armidale NSW Australia) was installed at a distal part of the branch to record xylem pressures for every 15 min. To obtain pressure estimates for each point in time and to reduce the impact of measurement uncertainty in the psychrometric water potentials, the psychrometer measurements for each sample were smoothed with shape-constrained additive models using monotone decreasing P-splines based on R package `scam` v. 1.2-8 (Pya, 2020).

Measurements of vulnerability curves with the flow-centrifuge method

The flow-centrifuge technique (Cavitron; Cochard *et al*., 2005) was used as a reference method for comparing the agreement of xylem vulnerability curves based on hydraulic measurement methods with curves based on the Pneumatron. Flow-centrifuge measurements were performed for 49 samples from 36 trees with a Cavitron device built from a Sorval RC 5 series centrifuge with manual control of rotation speed, and using the `Cavisoft` software (`Cavisoft` version 5.2.1, University of Bordeaux, Bordeaux, France). Samples were recut several times under

198 water to a final length of 27.5 cm to release the tension in the xylem (Torres-Ruiz *et al*., 2015).
199 Subsequently, the non-flushed branch segments were inserted in a custom-made rotor after
200 removing the bark at both ends. They were then spun using the principle of centrifugal force to
201 generate a negative pressure in the xylem segment while simultaneously measuring hydraulic
202 conductance. Flow centrifuge measurements were performed with filtered (0.2 µm) and
203 degassed demineralized water that was enriched with 10 mM KCl and 1 mM $CaCl_2$.
204 Measurements began at xylem water potentials of around -0.8 MPa and were continued under
205 increasingly negative xylem pressures until the percentage loss of hydraulic conductivity (PLC)
206 reached at least 90%.
207
208 *Statistical analysis*
209 All data handling and statistical analyses were performed in `R` version 4.0.2 (`R` Core Team,
210 2020) in the framework of the `tidyverse` (Wickham *et al*., 2019). Both the vulnerability
211 curves based on pneumatic and flow-centrifuge measurements were described with tree-level
212 nonlinear regression models using the logistic function by Pammenter & Van der Willigen
213 (1998). For the flow-centrifuge method, vulnerability curves were based on the raw
214 conductivity measured by the Cavitron (cf. Ogle *et al*., 2009):

215 $$K_i = \text{Normal}\left(k_{sat}\left(1 - \frac{1}{1+\exp\left(\frac{S_{50H}}{25}(\mathrm{P_i} - \mathrm{P_{50H}})\right)}\right), \sigma\right), \quad (2)$$

216 where K_i and P_i are the measured hydraulic conductivity and xylem pressure for observation *i*,
217 respectively, k_{sat} is the hydraulic conductivity under fully saturated conditions, and S_{50H} is the
218 slope at 50% loss of conductivity (P_{50H}). For the pneumatic measurements, analogous models
219 were constructed based on PAD for estimating P_{50P} (Eq. 1):

220 $$PAD_i = \text{Normal}\left(\frac{100}{1+\exp\left(\frac{S_{50P}}{25}(\mathrm{P_i} - \mathrm{P_{50P}})\right)}, \sigma\right), \quad (3)$$

To evaluate the effect of the air-discharge time on the accuracy of the estimates of vulnerability curve parameters, separate pneumatic vulnerability curves were fit on PAD calculated for all measurement durations between the initial pressure immediately after pumping and variable final pressures in 0.5 sec intervals, from 4.5 to 115 sec. The P_{12} and P_{88} (xylem pressure at 12% and 88% loss of conductivity, respectively) were calculated from the estimated model parameters (P_{50} and the corresponding slope at this pressure) by rearranging the model equation (Eqs. 2 & 3), and with confidence intervals based on parametric bootstrap (n = 10,000). The uncertainty in VC parameters was taken into account for the calculation of species averages of VC parameters and their standard errors by using inverse-variance weighting analogous to a fixed-effects meta-analytical model (cf. Rosenberg *et al*., 2013).

We subsequently calculated a set of statistics that describe the degree of agreement of the Pneumatron parameter estimates with the flow-centrifuge based values in terms of systematic deviations, random deviations, and overall agreement. For the Pneumatron measurements from *Tilia japonica*, *T. cordata* and *T. platyphyllos*, these calculations were based on tree averages of the flow-centrifuge parameters when replicate measurements were performed per tree (Tab. 1).

Systematic deviations between Pneumatron and flow-centrifuge based VC parameter estimates were quantified by the mean signed deviation (MSD). The MSD only measures additive bias between the parameter estimates obtained by the pneumatic and flow-centrifuge methods (θ_P and θ_H, respectively) and does not penalize scatter in the relationship.

$$\mathrm{MSD} = \frac{1}{n}\sum(\theta_P - \theta_H) \quad (5)$$

Random deviations between the estimates of both methods was evaluated by the Pearson correlation ρ between θ_P and θ_H. The correlation coefficient only penalizes the degree of scatter around a hypothetical line through θ_P and θ_H and does not include information about systematic differences.

$$\rho = \frac{\mathrm{cov}(\theta_P,\theta_H)}{\mathrm{SD}(\theta_p)\,\mathrm{SD}(\theta_H)} \quad (4)$$

The overall agreement of the parameter estimates was evaluated by the root mean square deviation (RMSD). Unlike the aforementioned metrics, the RMSD penalizes both systematic and random deviations between θ_P and θ_H.

$$\mathrm{RMSD} = \sqrt{\frac{1}{n}\sum(\theta_P - \theta_H)^2} \quad (6)$$

In addition, as a pragmatic measure to quantify the overall match of the flow-centrifuge and pneumatic vulnerability curves over their entire range, we calculated the L_2 distance (cf. Cramér, 1928) between each pair of flow-centrifuge and pneumatic vulnerability curves:

$$L_2 = \left(\int_{-\infty}^{\infty} \left(PLC_H(P) - PLC_P(P)\right)^2 \mathrm{dP}\right)^{1/2} \quad (7)$$

This quantity describes the degree of similarity of the two vulnerability curves and approaches zero for identical curves.

In addition to the comparison of metrics describing the agreement between estimates, we used linear mixed effects models based on R package `lme4` version 1.1-23 (Bates *et al*., 2015) to test for statistically significant differences between the Cavitron-based estimates of P_{12}, P_{50}, P_{88} and (natural log-transformed) S_{50} and their Pneumatron-based equivalents for AD intervals of 15, 30, 60, 90 and 115 sec from the initial pressure at 4 sec. Each model was fit to each parameter using restricted maximum likelihood with "method" as a fixed effect and random intercepts for species and individual trees nested in species. The flow-centrifuge was considered as baseline and contrasted with each one term for the Pneumatron estimates in five different intervals. Model assumptions were checked by residual diagnostic plots. Inference was based on Wald *t*-tests with Sattherthwaite's approximation to the degrees of freedom using R package `lmerTest` version 3.1-2 (Kuznetsova *et al*., 2017).

Results

Estimated vulnerability curves

The average P_{50H} estimates obtained from the flow-centrifuge method covered a wide range of embolism resistance from -1.85 MPa to -6.02 MPa for *Platanus* × *acerifolia* and *Crataegus persimilis*, respectively. Parameters estimated with the pneumatic method largely fell into the same range (cf. Table S1). In general, there was a good agreement in overall shape between the flow-centrifuge and pneumatic vulnerability curves (VCs) for most of the species studied. However, the estimates in P_{12P}, P_{50P} and P_{88P} for *T. cordata* and *T. platyphyllos* based on the pneumatic method were on average at least 0.5 MPa higher than the corresponding estimates of the flow-centrifuge method when their xylem pressure was measured using a pressure chamber (Table S1). Additional measurements performed to explain this discrepancy showed that embolism resistance was largely within a comparable range when xylem pressure was determined by stem psychrometers (with the exception of P_{88P} for *T. cordata*; Table S1; Fig. S4). As there were reasons to assume that the differences observed were caused by inaccurate xylem water potential measurements with the pressure chamber, results for the best AD measurement intervals are based only on the observations with xylem pressure measurements based on stem psychrometers.

Overall agreement between methods

The parameters of the vulnerability curves estimated with the two methods were generally highly correlated, with Pearson correlations above 0.54 for all parameters and over 0.74 for P_{12}, P_{50} and P_{88} for all AD times considered in Table S2 and all 12 tree species (Table S2). In particular, this was true for the P_{50} estimates, where correlations exceeded 0.95 in all cases. Moreover, the P_{50} estimates of the two methods were very close to the 1:1 line (cf. Fig. 2b, Table S2). The Pneumatron-based estimates of the slope of the vulnerability curve, however, on average showed a negative systematic deviation that ranged from −25.5% (retransformed

295 from log scale, 15 sec AD time) to −28.1% (115 sec AD time; cf. Fig. 1, 2d; Table S2). The
296 deviation was notably larger in samples with lower slopes, and was not observed for the samples
297 measured with stem psychrometers (Fig. 2). Due to the direct relationship between slope and
298 P_{50}, the systematically lower slope estimates translated to a higher P_{12P} (by up to 0.77 MPa on
299 average at 115 sec AD time) and, in some cases, a lower P_{88P} (by up to −0.26 MPa on average
300 at 15 sec AD time; Fig. 2, Table S2).
301
302 *Influence of discharge time*
303 The pneumatic estimates of all VC parameters were sensitive to the chosen discharge time
304 (Table 2, S2, Fig. 3, 4, 5). However, the change in agreement with air discharge time was neither
305 consistent between parameters nor between species (Table S2, Fig. 4, 5). Consequently, the
306 discharge interval associated with the lowest deviation between flow-centrifuge and pneumatic
307 estimates of P_{50} (Fig. 3) and other parameters differed largely between species, with an
308 increasing deviation with discharge time for some species (*Betula, Carpinus, Crataegus* and
309 *Tilia*) and a decreasing deviation for others (*Ostrya, Platanus, Pyrus* and *Sorbus*). After
310 accounting for random variation between species and trees, significant systematic differences
311 between the reference value based on the flow-centrifuge method and the pneumatic method at
312 all analysed AD times remained for all parameters, with the exception of P_{88} (Table 2).
313 The response of the pneumatic estimates of the vulnerability curve parameters to AD time was
314 not consistent between parameters (Fig. 4). Depending on the parameter, the overall agreement
315 with the flow-centrifuge method was either highest at low AD times (P_{12}), remained relatively
316 stable over a wide range of AD times (P_{50}, S_{50}) or increased continuously with increasing AD
317 time (P_{88}; cf. Fig. 4). In any case, the L_2 distance (which describes the overall match of the
318 curves over their entire range instead of focusing on a point estimate) was lowest at relatively
319 low AD times with a minimum at 16 sec and a relatively broad range of equivalent values from
320 10.5 to 44.5 sec (Fig. 5). This indicates that the lowest degree of dissimilarity between the

321 curves corresponded to AD times in this range, which moreover was associated with the lowest
322 systematic differences in P_{50} estimates (Table 2, S2; Fig. 4).
323
324 **Discussion**
325 In agreement with previous assessments of the pneumatic method for vulnerability curve (VC)
326 measurements (Pereira *et al*., 2016, 2020; Zhang *et al*., 2018; Sergent *et al*., 2020), we find that
327 the estimated water potential at 50% of discharged air volume (P_{50P}) coincide well with the
328 water potential at 50% loss of conductance (P_{50H}) measured with the flow-centrifuge method
329 for the 12 diffuse-porous temperate tree species studied, with low systematic and random
330 deviations and a high overall agreement (MSD = +0.117 MPa, ρ = 0.956, RMSD = ±0.538
331 MPa, respectively for 15 sec AD time, Table S2). However, we find evidence for a high
332 variance and systematic differences in the estimates of the slope of the VC (Fig. 1), that were
333 on average at least 25.5% (15 sec air discharge time, cf. Table S2) lower for the pneumatic
334 method, which also resulted in a lower agreement in the estimates of P_{12P} and P_{88P}. Similar
335 conclusions were found based on a pneumatic modelling approach (Yang *et al*., 2021), and
336 based on experimental evidence by comparing the pneumatic and the optical method (Pereira
337 *et al*., 2020; Guan *et al*., 2021). A mechanistic explanation for the difference in P_{12} and P_{88}
338 values is provided by the open-xylem artefact, which suggests that embolism spreading could
339 be enhanced by the proximity to gas under atmospheric pressure in the open-cut conduits (Guan
340 *et al*., 2021).
341 Moreover, our results demonstrate that the estimates obtained with the pneumatic method are
342 sensitive to the choice of air discharge time (cf. Pereira *et al*., 2016, 2020), to which they
343 respond in a nonlinear and species-specific manner. For the analyzed set of species, the best
344 overall match between the flow-centrifuge and pneumatic VCs could be achieved for air
345 discharge times of around 15 sec (cf. Fig. 4), which experimentally confirms the ideal AD time
346 identified by a modelling approach (Yang *et al*., 2021).

347

348 *Agreement between flow-centrifuge and pneumatic vulnerability curves*

349 The gradual loss of conductance and the increasing amount of gas extracted, which are
350 quantified by the PLC and PAD, are necessarily positively associated as they share a common
351 cause, namely embolism spreading under progressing dehydration. However, PAD quantifies
352 the air volume inside embolised vessels, while PLC measures their contribution to the
353 conductance of the branch. Thus, both arise from vessel properties that scale with different
354 powers of their length and diameter (Pereira *et al*., 2016). While the volume of a vessel scales
355 with the second power of diameter and is proportional to its length, its flow resistance (i.e. the
356 inverse of its conductance) can be approximated by the sum of the resistance posed by its lumen
357 and the resistance posed by the transition through pit membranes (Sperry *et al*., 2005; Wheeler
358 *et al*., 2005). According to the Hagen-Poseuille-equation, the flow resistance of the lumen
359 scales with the inverse of the fourth power of its diameter and is proportional to its length. The
360 flow resistance posed by the transition through pit membranes can be assumed to scale with the
361 inverse of expected vessel length (Sperry *et al*., 2005). Due to these different scaling
362 relationships, the association between PAD and PLC does not necessarily have to be linear.
363 Observed systematic differences between the parameters of curves obtained with different
364 methods (cf. Table 2) might therefore not be surprising and deserve further testing.
365 It should also be noted that an additional downward bias in the slope might be introduced by
366 treating the unknown true minimum and maximum amount of air discharged (AD_{min} and AD_{max},
367 cf. Eq. 1) as fixed quantities measured without error. For hydraulic vulnerability curves,
368 problems induced by treating maximum conductivity as fixed can be circumvented by treating
369 the saturated hydraulic conductivity as a model parameter (k_{sat} in Eq. 2; Ogle *et al*., 2009;
370 Duursma & Choat, 2017). Implementing a similar solution for the pneumatic method is not
371 straightforward due to the common identifiability issues in sigmoidal models where the lower
372 and upper bound are both treated as model parameters.

Given the direct mathematical relation between the model parameters, a bias in slope can be expected to result in a bias in P_{12} and/or P_{88}, which may be problematic in process-based vegetation modelling that use these VC parameters to describe drought resistance. Our results indicate that while the pneumatic method produces reliable estimates of the P_{50} for diffuse-porous tree species, the curves obtained might not always be interchangeable with curves constructed with the flow-centrifuge method.

Effect of the air discharge interval on measurement accuracy

The observed sensitivity of the pneumatic method to the AD interval provides experimental evidence that is in line with predictions by the Unit Pipe Pneumatic model (Yang *et al*., 2021). To understand the relationship between the AD interval and the amount of air discharged in that interval, it is necessary to focus on the underlying assumptions about the gas flow between sample and reservoir. One central assumption of the pneumatic method is that the amount of air discharged into the vacuum reservoir over a given time span is a function of the amount of air N inside embolised conduits at different points during the dehydration process (Jansen *et al*., 2020; Yang *et al*.,2021). This assumption is necessary to be able to use PAD measurements to infer the degree of embolization. Further, if the PAD calculated over different AD times t is to result in identical vulnerability curves, the change in AD with time must have the same shape at different dehydration steps and only differ by a multiplicative constant proportional to the amount of air N in the xylem, i.e. $\mathrm{AD}(t, N_1) / N_1 = \mathrm{AD}(t, N_2) / N_2$ must hold. This assumption is likely only approximately met under typical measurement conditions. During the drying process, the xylem undergoes substantial changes that may affect the shape of $\mathrm{AD}(t, N)$, such as an increase in gas conductivity with progressing embolism. Moreover, it is possible that embolised conduits that were not disconnected from to the cut surface at earlier drying steps subsequently become connected to the network of open vessels connecting to the vacuum reservoir (Pereira et al. 2016). In such cases, the amount of air in these spaces would not be

399 included in the earlier estimates. For these reasons, the relationship between the AD measured
400 in different desiccation steps after a certain discharge interval and the total amount of air within
401 the xylem at those points in time is likely empirical. This may explain the pronounced species
402 differences in the response to AD time (Table S2, 4, Fig. 3), and contribute to the previously
403 reported differences in accuracy for species with different types of wood anatomy (e.g. Zhang
404 *et al*., 2018).
405 While the effect of AD time depended on species identity, and was different for different
406 parameters, Fig. 4 indicates that overall mismatch between flow-centrifuge and pneumatic VCs
407 could be minimized by choosing low AD times of ca.16 sec. In our setting, this might be a
408 consequence of small amounts of air-entry into the xylem where the branch is damaged, which
409 – unlike the other discussed factors influencing AD – will have an effect that accumulates with
410 discharge time. Thus, the net gains in accuracy due to integrating over a larger time interval are
411 overcompensated by the increasing contribution of potential leakage to the total AD.
412 Interestingly, the higher agreement with hydraulic reference values at lower AD times contrasts
413 with the higher accuracy for longer AD times reported in earlier works using the manual
414 pneumatic method (cf. Fig. S3 in Pereira et al. 2016). Most likely, this difference results from
415 the higher temporal resolution and more accurate AD time measurement enabled by the
416 automated Pneumatron device (Pereira et al. 2020). When using a Pneumatron, the choice of
417 short AD times therefore is a pragmatic way to improve the accuracy of the pneumatic method.
418
419 *Species-specific drying behaviour*
420 As noted previously (Zhang *et al*., 2018; Sergent *et al*., 2020), the degree of similarity between
421 VCs measured with the pneumatic method and hydraulic reference methods differs between
422 species. In this study, we observed a mismatch for *T. cordata* and *T. platyphyllos* when xylem
423 pressure was expressed based on leaf water potentials measured with a pressure chamber.

However, the difference largely disappeared when a stem psychrometer was used to determine xylem pressure (Fig. 1, S4).

Possible explanations for the observed differences is the presence of abundant mucilage in the xylem tissues of *Tilia* species (Franz & Kram, 1985; Pigott *et al*., 2012), which has been reported to affect xylem pressures measured with the pressure chamber technique (Zimmermann *et al*., 2002). Furthermore, it could be speculated that the truncated shape of the pressure-chamber based Pneumatron VCs for the *Tilia* species (especially *T. cordata*, cf. Fig. S4), and the fact they never reached water potentials substantially more negative than -3 MPa, indicates that the measurements were terminated before the stems of the specimens were fully dehydrated. This results in underestimated values for AD_{max}, thus shifting the curve towards less negative water potentials. As detailed before, the desiccation was continued until a near constancy in the measured *AD* values over at least 24 h was reached. This criterion to finish *AD* measurements may not be ideal, as the drying process may slow down notably after full stomatal closure, which especially for isohydric species may happen in a relatively well-hydrated state. Notably, while *Tilia* species have often been considered to be relatively anisohydric (cf. Leuzinger *et al*., 2005; Galiano *et al*., 2017; Kiorapostolou *et al*., 2018; but see Niinemets *et al*., 1999), recent work by Leuschner *et al*. (2019) indicates that at least *T. cordata* has a fairly stringent, more isohydric stomatal control mechanism. Due to the anticipated hydraulic segmentation between leaf petioles and stem xylem in drought-avoiding and more isohydric species (Hartmann *et al*., 2021), this may have contributed to the mismatch between flow-centrifuge and pneumatic VCs. It is well documented that certain species rely on early drought-induced leaf shedding (Wolfe *et al*., 2016; Hochberg *et al*., 2017), most likely caused by a pronounced hydraulic segmentation (cf. Pivovaroff *et al*., 2016; Zhu *et al*., 2016; Klepsch *et al*., 2018). As these processes decouple leaf and branch water potentials, measuring leaf water potential with a Scholander pressure chamber may result in extreme water potential readings that do not reflect the actual status in the xylem. Conversely, the slowdown of dehydration

450 induced by leaf shedding may result in prematurely terminated measurements when measuring
451 branch water potentials with e.g. a stem psychrometer, or when determining the end of the
452 dehydration process based on the state of the leaves. As a cautionary example, the leaves of
453 *C. persimilis* were almost fully dehydrated on the third day of measurements, while the branch
454 water potential values continued to decline for seven days. Similar behaviour was reported by
455 Wolfe *et al*. (2016) for the tropical species *Genipa americana*.
456 Due to these species-specific differences in drying behaviour, the stability of AD_{max} can have a
457 strong influence on the shape of the vulnerability curves because all pneumatic *PAD* values are
458 normalized against AD_{min} and AD_{max}. It may therefore be advantageous to continue the drying
459 process until the constancy of AD_{max} has been confirmed based on several measurements to
460 avoid bias resulting from underestimating AD_{max}. An important corollary of the observed
461 problems associated with water potential measurements is that the same kind of bias in water
462 potential may also affect hydraulic VC measurements in other methods that rely on bench
463 dehydration.
464
465 *Implications for future vulnerability curve method comparisons*
466 An important limitation that affects all evaluation studies of VC methods – as well as most
467 other measurement methods in biology – is the lack of true reference values for VC parameters.
468 While in this study, we used measurements with the flow-centrifuge method as a reference,
469 there are many indications that this method may be affected by measurement artefacts that arise
470 during sample excision (Wheeler *et al*., 2013) and preparation (Torres-Ruiz *et al*., 2015) or as
471 a result from vessel lengths exceeding the sample dimensions (Choat *et al*., 2010; Martin-StPaul
472 *et al*., 2014; Torres-Ruiz *et al*., 2014). A mismatch between curves obtained with the pneumatic
473 method and the flow-centrifuge method may thus in part also be attributed to the imperfections
474 of the latter. While there is hardly a way to overcome the limitation of imperfect reference
475 values, we argue that methodological comparisons of VC methods may benefit from adopting

476 a more principled approach of quantifying the agreement between different methods in terms
477 of different components of accuracy (cf. Fuchs *et al*., 2017; Flo *et al*., 2019). To our knowledge,
478 none of the previously published methodological comparisons (see e.g. Li *et al*., 2008; Choat
479 *et al*., 2010; Hacke *et al*., 2015; Brodribb *et al*., 2017; López *et al*., 2019; Venturas *et al*., 2019;
480 Chen *et al*., 2021; Pratt *et al*., 2020; Sergent *et al*., 2020; Zhao *et al*., 2020) formally differentiate
481 between systematic and random differences in parameter estimates, and none provide metrics
482 that quantify the similarity over the entire curves. While our choice of the L_2-distance as a
483 measure of overall agreement between curves is relatively arbitrary and there are many equally
484 appropriate distance metrics, it is most definitely an improvement compared to the common
485 practice of comparing methods by the Pearson correlation between parameter estimates, as the
486 latter only penalizes deviations from a bivariate linear relationship while being insensitive to
487 systematic deviations. We hope that our framework can serve as a starting point for more formal
488 VC method comparisons based on rigorous metrological principles and theory.
489
490 *Conclusions*
491 Our data indicate a high degree of agreement between the P_{50P} estimated with the pneumatic
492 method and the P_{50H} estimated with the flow-centrifuge method for the analysed diffuse-porous
493 temperate tree species, especially when using short air discharge times of around 15 sec. The
494 relatively low effort required to construct a curve with this method and its high degree of
495 automation when using a Pneumatron device in conjunction with a stem psychrometer allow
496 for a high throughput. The method is therefore attractive in descriptive or predictive contexts
497 where the main purpose is to generate a good proxy for plant drought resistance. However, the
498 observed systematic deviation in slope estimates as well as potential artefacts associated with
499 xylem water potential determination and species-specific drying behaviour deserve further
500 attention.
501

Acknowledgements

We thank Klaus Körber and Andreas Lösch from the Bavarian state institute for viticulture and horticulture (Bayerische Landesanstalt für Wein- und Gartenbau, LWG) for granting access to their research facility at Stutel and Xinyi Guan for her support with the automated pneumatic measurements. P.R.L.B. acknowledges Royal Society's Newton International for its Fellowship (NF170370). S.J. acknowledges funding from the German Research Foundation (Deutsche Forschungsgemeinschaft, DFG, project nr. 410768178).

Author contributions

B.S. and R.M.L. designed the study, S.S.P. performed the semi-automated pneumatic measurements, technically supported by P.B. and L.P., L.P. the automated pneumatic measurements and E.I. the hydraulic measurements. S.S.P. and R.M.L. analysed the data. S.S.P, R.M.L. and B.S. wrote the first manuscript, which was intensively discussed and revised by all authors.

References

Adams HD, Zeppel MJB, Anderegg WRL, Hartmann H, Landhäusser SM, Tissue DT, Huxman TE, Hudson PJ, Franz TE, Allen CD, *et al*. 2017. A multi-species synthesis of physiological mechanisms in drought-induced tree mortality. *Nature Ecology & Evolution* **1**: 1285–1291.

Allen CD, Breshears DD, McDowell NG. 2015. On underestimation of global vulnerability to tree mortality and forest die-off from hotter drought in the Anthropocene. *Ecosphere* **6**: 1–55.

Allen CD, Macalady AK, Chenchouni H, Bachelet D, McDowell N, Vennetier M, Kitzberger T, Rigling A, Breshears DD, Hogg EH (Ted), *et al*. 2010. A global overview of drought and heat-induced tree mortality reveals emerging climate change risks for forests. *Forest Ecology and Management* **259**: 660–684.

Anderegg WRL, Klein T, Bartlett M, Sack L, Pellegrini AFA, Choat B, Jansen S. 2016. Meta-analysis reveals that hydraulic traits explain cross-species patterns of drought-induced tree mortality across the globe. *Proceedings of the National Academy of Sciences* **113**: 5024–5029.

Bates D, Mächler M, Bolker B, Walker S. 2015. Fitting linear mixed-effects models using lme4. *Journal of Statistical Software* **67**: 1–48.

Bittencourt PRL, Pereira L, Oliveira RS. 2018. Pneumatic Method to Measure Plant Xylem Embolism. *Bio-Protocol* **8**.

Blackman CJ, Gleason SM, Chang Y, Cook AM, Laws C, Westoby M. 2014. Leaf hydraulic vulnerability to drought is linked to site water availability across a broad range of species and climates. *Annals of Botany* **114**: 435–440.

Brando PM, Paolucci L, Ummenhofer CC, Ordway EM, Hartmann H, Cattau ME, Rattis L, Medjibe V, Coe MT, Balch J. 2019. Droughts, Wildfires, and Forest Carbon Cycling: A Pantropical Synthesis. *Annual Review of Earth and Planetary Sciences* **47**: 555–581.

Brodersen CR, McElrone AJ, Choat B, Matthews MA, Shackel KA. 2010. The Dynamics of Embolism Repair in Xylem: In Vivo Visualizations Using High-Resolution Computed Tomography. *Plant Physiology* **154**: 1088–1095.

Brodribb TJ, Cochard H. 2009. Hydraulic Failure Defines the Recovery and Point of Death in Water-Stressed Conifers. *Plant Physiology* **149**: 575–584.

Brodribb TJ, Skelton RP, McAdam SA, Bienaimé D, Lucani CJ, Marmottant P. 2016. Visual quantification of embolism reveals leaf vulnerability to hydraulic failure. *New Phytologist* **209**: 1403–1409.

Brodribb TJ, Carriqui M, Delzon S, Lucani C. 2017. Optical Measurement of Stem Xylem Vulnerability. *Plant Physiology* **174**: 2054–2061.

549 **Brodribb TJ, Powers J, Cochard H, Choat B. 2020.** Hanging by a thread? Forests and drought.
550 *Science* **368**: 261–266.**Chen Y, Maenpuen P, Zhang Y, Barai K, Katabuchi M, Gao H,**
551 **Kaewkamol S, Tao L, Zhang J. 2020.** Quantifying vulnerability to embolism in tropical trees
552 and lianas using five methods: can discrepancies be explained by xylem structural traits? *New*
553 *Phytologist* **229**: 805–819.

554 **Chen Y, Maenpuen P, Zhang Y, Barai K, Katabuchi M, Gao H, Kaewkamol S, Tao L, Zhang J.**
555 **2021.** Quantifying vulnerability to embolism in tropical trees and lianas using five methods: can
556 discrepancies be explained by xylem structural traits? *New Phytologist* **229**: 805–819.

557 **Choat B, Drayton WM, Brodersen C, Matthews MA, Shackel KA, Wada H, Mcelrone AJ. 2010.**
558 Measurement of vulnerability to water stress-induced cavitation in grapevine: a comparison of
559 four techniques applied to a long-vesseled species: Comparison of vulnerability curve technique
560 in grapevine. *Plant, Cell & Environment* **491**: 752-755.

561 **Choat B, Jansen S, Brodribb TJ, Cochard H, Delzon S, Bhaskar R, Bucci SJ, Feild TS, Gleason**
562 **SM, Hacke UG *et al*. 2012.** Global convergence in the vulnerability of forests to drought. *Nature*
563 **491**: 752–755.

564 **Choat B, Brodribb TJ, Brodersen CR, Duursma RA, López R, Medlyn BE. 2018.** Triggers of tree
565 mortality under drought. *Nature* **558**: 531–539.

566 **Christoffersen BO, Gloor M, Fauset S, Fyllas NM, Galbraith DR, Baker R, Kruijt B, Rowland L,**
567 **Fisher RA, Binks OJ *et al*. 2016.** Linking hydraulic traits to tropical forest function in a size-
568 structured and trait-driven model (TFS v.1-Hydro). *Geoscientific Model Development* **9**: 4227–
569 4255.

570 **Cochard H, Cruiziat P, Tyree MT. 1992.** Use of Positive Pressures to Establish Vulnerability Curves.
571 *Plant Physiology* **100**: 205–209.

572 **Cochard H, Damour G, Bodet C, Tharwat I, Poirier M, Améglio T. 2005.** Evaluation of a new
573 centrifuge technique for rapid generation of xylem vulnerability curves. *Physiologia Plantarum*
574 **124**: 410–418.

575 **Cochard H, Badel E, Herbette S, Delzon S, Choat B, Jansen S. 2013.** Methods for measuring plant
576 vulnerability to cavitation: a critical review. *Journal of Experimental Botany* **64**: 4779–4791.

577 **Correia DLP, Bouchard M, Filotas É, Raulier F. 2019.** Disentangling the effect of drought on stand
578 mortality and productivity in northern temperate and boreal forests. *Journal of Applied Ecology*
579 **56**: 758–768.

580 **Cramér H. 1928.** On the composition of elementary errors. II Statistical applications. *Skandinavisk*
581 *Aktuarietidskrift* **11**: 141–180.

582 **Davi H, Cailleret M. 2017.** Assessing drought-driven mortality trees with physiological process-based
583 models. *Agricultural and Forest Meteorology* **232**: 279–290.

584 **Delzon S, Cochard H. 2014.** Recent advances in tree hydraulics highlight the ecological significance
585 of the hydraulic safety margin. *New Phytologist* **203**: 355–358.

586 **Duursma RA, Choat B. 2017.** fitplc : an R package to fit hydraulic vulnerability curves. *Journal of*
587 *Plant Hydraulics* **4**: e002.

588 **Eller CB, Rowland L, Mencuccini M, Rosas T, Williams K, Harper A, Medlyn BE, Wagner Y,**
589 **Klein T, Teodoro GS, *et al.* 2020.** Stomatal optimization based on xylem hydraulics (SOX)
590 improves land surface model simulation of vegetation responses to climate. *New Phytologist* **226**:
591 1622–1637.

592 **Field CB, Barros V, Stocker TF, Dahe Q (Eds.). 2012.** Managing the Risks of Extreme Events and
593 Disasters to Advance Climate Change Adaptation: Special Report of the Intergovernmental Panel
594 on Climate Change. Cambridge: *Cambridge University Press*.

595 **Flo V, Martinez-Vilalta J, Steppe K, Schuldt B, Poyatos R. 2019.** A synthesis of bias and uncertainty
596 in sap flow methods. *Agricultural and Forest Meteorology* **271**: 362–374.

597 **Franz G, Kram G. 1985.** Structural investigations on the watersoluble polysaccharides of lime tree
598 flowers. *Die Pharmazie* **41**: 501.

599 **Fuchs S, Leuschner C, Link R, Coners H, Schuldt B. 2017.** Calibration and comparison of thermal
600 dissipation, heat ratio and heat field deformation sap flow probes for diffuse-porous trees.
601 *Agricultural and Forest Meteorology* **244–245**: 151–161.

602 **Galiano L, Timofeeva G, Saurer M, Siegwolf R, Martínez-Vilalta J, Hommel R, Gessler A. 2017.**
603 The fate of recently fixed carbon after drought release: towards unravelling C storage regulation
604 in *Tilia platyphyllos* and *Pinus sylvestris*. *Plant, Cell & Environment* **40**: 1711–1724.

605 **Guan X., Pereira L., McAdam S.A.M., Cao K., Jansen S. 2021.** No gas source, no problem: proximity
606 to pre-existing embolism and segmentation affect embolism spreading in angiosperm xylem by
607 gas diffusion. *Plant, Cell & Environment*. doi: 10.1111/pce.14016.

608 **Hacke UG, Venturas MD, MacKinnon ED, Jacobsen AL, Sperry JS, Pratt RB. 2015.** The standard
609 centrifuge method accurately measures vulnerability curves of long-vesselled olive stems. *New*
610 *Phytologist* **205**: 116–127.

611 **Hartmann H, Link RM, Schuldt B. 2021.** A whole-plant perspective of isohydry: stem-level support
612 for leaf-level plant water regulation. *Tree Physiology*, accepted.

613 **Hochberg U, Windt CW, Ponomarenko A, Zhang Y-J, Gersony J, Rockwell FE, Holbrook NM.**
614 **2017.** Stomatal Closure, Basal Leaf Embolism, and Shedding Protect the Hydraulic Integrity of
615 Grape Stems. *Plant Physiology* **174**: 764–775.

Jansen S, Schuldt B, Choat B. 2015. Current controversies and challenges in applying plant hydraulic techniques. *New Phytologist* **205**: 961–964.

Jansen S, Guan X, Kaack L, Trabi C, Miranda M, Ribeiro R, Pereira L. 2020. The Pneumatron estimates xylem embolism resistance in angiosperms based on gas diffusion kinetics: a mini-review. *Acta Horticulturae* **1300**: 193–200.

Kiorapostolou N, Galiano-Pérez L, von Arx G, Gessler A, Petit G. 2018. Structural and anatomical responses of *Pinus sylvestris* and *Tilia platyphyllos* seedlings exposed to water shortage. *Trees* **32**: 1211–1218.

Klepsch M, Zhang Y, Kotowska MM, Lamarque LJ, Nolf M, Schuldt B, Torres-Ruiz JM, Qin D-W, Choat B, Delzon S, *et al*. 2018. Is xylem of angiosperm leaves less resistant to embolism than branches? Insights from microCT, hydraulics, and anatomy. *Journal of Experimental Botany* **69**: 5611–5623.

Kuznetsova A, Brockhoff PB, Christensen RHB. 2017. lmerTest Package: Tests in Linear Mixed Effects Models. *Journal of Statistical Software* **82**: 1–26.

Leuschner C, Wedde P, Lübbe T. 2019. The relation between pressure–volume curve traits and stomatal regulation of water potential in five temperate broadleaf tree species. *Annals of Forest Science* **76**: 60.

Leuzinger S, Zotz G, Asshoff R, Korner C. 2005. Responses of deciduous forest trees to severe drought in Central Europe. *Tree Physiology* **25**: 641–650.

Li Y, Sperry JS, Taneda H, Bush SE, Hacke UG. 2008. Evaluation of centrifugal methods for measuring xylem cavitation in conifers, diffuse- and ring-porous angiosperms. *New Phytologist* **177**: 558–568.

López R, Nolf M, Duursma RA, Badel E, Flavel RJ, Cochard H, Choat B. 2019. Mitigating the open vessel artefact in centrifuge-based measurement of embolism resistance (R Tognetti, Ed.). *Tree Physiology* **39**: 143–155.

Martin-StPaul NK, Longepierre D, Huc R, Delzon S, Burlett R, Joffre R, Rambal S, Cochard H. 2014. How reliable are methods to assess xylem vulnerability to cavitation? The issue of 'open vessel' artifact in oaks. *Tree Physiology* **34**: 894–905.

Martin-StPaul N, Delzon S, Cochard H. 2017. Plant resistance to drought depends on timely stomatal closure. *Ecology Letters* **20**: 1437–1447.

McDowell NG, Fisher RA, Xu C, Domec JC, Hölttä T, Mackay DS, Sperry JS, Boutz A, Dickman L, Gehres N *et al*. 2013a. Evaluating theories of drought-induced vegetation mortality using a multimodel-experiment framework. *New Phytologist* **200**: 304–321.

649 **McDowell NG, Ryan MG, Zeppel MJB, Tissue DT. 2013b.** Feature: Improving our knowledge of
650 drought-induced forest mortality through experiments, observations, and modeling. *New*
651 *Phytologist* **200**: 289–293.

652 **Meinzer FC, Johnson DM, Lachenbruch B, McCulloh KA, Woodruff DR. 2009.** Xylem hydraulic
653 safety margins in woody plants: coordination of stomatal control of xylem tension with hydraulic
654 capacitance. *Functional Ecology* **23**: 922–930.

655 **Niinemets Ü, Sõber A, Kull O, Hartung W, Tenhunen JD. 1999.** Apparent Controls on Leaf
656 Conductance by Soil Water Availability and via Light-Acclimation of Foliage Structural and
657 Physiological Properties in a Mixed Deciduous, Temperate Forest. *International Journal of Plant*
658 *Sciences* **160**: 707–721.

659 **Nolf M, López R, Peters J, Flavel R, Koloadin L, Young I, Choat B. 2017.** Visualization of xylem
660 embolism by X-ray microtomography: A direct test against hydraulic measurements. *New*
661 *Phytologist* **214**: 890–898.

662 **Ogle K, Barber JJ, Willson C, Thompson B. 2009.** Hierarchical statistical modeling of xylem
663 vulnerability to cavitation. *New Phytologist* **182**: 541–554.

664 **Oliveira RS, Costa FRC, Baalen E van, Jonge A de, Bittencourt PR, Almanza Y, Barros F de V,**
665 **Cordoba EC, Fagundes MV, Garcia S *et al*. 2019.** Embolism resistance drives the distribution
666 of Amazonian rainforest tree species along hydro-topographic gradients. *New Phytologist* **221**:
667 1457–1465.

668 **Pammenter NW, Vander Willigen C. 1998.** A mathematical and statistical analysis of the curves
669 illustrating vulnerability of xylem to cavitation. *Tree Physiology* **18**: 589–593.

670 **Pereira L, Bittencourt PRL, Oliveira RS, Junior MBM, Barros FV, Ribeiro RV, Mazzafera P.**
671 **2016.** Plant pneumatics: stem air flow is related to embolism - new perspectives on methods in
672 plant hydraulics. *New Phytologist* **211**: 357–370.

673 **Pereira L, Bittencourt PRL, Pacheco VS, Miranda MT, Zhang Y, Oliveira RS, Groenendijk P,**
674 **Machado EC, Tyree MT, Jansen S *et al*. 2020.** The Pneumatron: An automated pneumatic
675 apparatus for estimating xylem vulnerability to embolism at high temporal resolution. *Plant, Cell*
676 *& Environment* **43**: 131–142.

677 **Pigott D. 2012.** Lime-trees and Basswoods: A Biological Monograph of the Genus *Tilia*. *Cambridge*
678 *University Press*.

679 **Pivovaroff AL, Burlett R, Lavigne B, Cochard H, Santiago LS, Delzon S. 2016.** Testing the
680 'microbubble effect' using the Cavitron technique to measure xylem water extraction curves. *AoB*
681 *Plants* **8**.

Powers JS, Vargas-G G, Brodribb TJ, Schwartz NB, Perez-Aviles D, Smith-Martin CM, Becknell JM, Aureli F, Blanco R, Calderón-Morales E *et al*. 2020. A catastrophic tropical drought kills hydraulically vulnerable tree species. *Global Change Biology* **26**: 3122–3133.

Pratt RB, Castro V, Fickle JC, Jacobsen AL. 2020. Embolism resistance of different aged stems of a California oak species (*Quercus douglasii*): optical and microCT methods differ from the benchtop-dehydration standard (M Ball, Ed.). *Tree Physiology* **40**: 5–18.

Pya N. 2020. scam: Shape Constrained Additive Models. R package version 1.2-8. URL: https://CRAN.R-project.org/package=scam

R Core Team. 2020. R: A language and environment for statistical computing. Vienna, Austria.

Rosenberg MS, Koricheva J, Gurevitch J, Mengersen K. 2013. Moment and least-squares based approaches to meta-analytic inference. In: Handbook of meta-analysis in ecology and evolution. Princeton and Oxford: *Princeton University Press*, 108–124.

Rosner S, Heinze B, Savi T, Dalla-Salda G. 2019. Prediction of hydraulic conductivity loss from relative water loss: new insights into water storage of tree stems and branches. *Physiologia Plantarum* **165**: 843–854.

Sergent AS, Varela SA, Barigah TS, Badel E, Cochard H, Dalla-Salda G, Delzon S, Fernández ME, Guillemot J, Gyenge J *et al*. 2020. A comparison of five methods to assess embolism resistance in trees. *Forest Ecology and Management* **468**: 118175.

Sperry JS, Donnelly JR, Tyree MT. 1988. A method for measuring hydraulic conductivity and embolism in xylem. *Plant, Cell & Environment* **11**: 35–40.

Sperry JS, Tyree MT. 1988. Mechanism of Water Stress-Induced Xylem Embolism. *Plant Physiology* **88**: 581–587.

Sperry JS, Hacke UG, Wheeler JK. 2005. Comparative analysis of end wall resistivity in xylem conduits. *Plant, Cell & Environment* **28**: 456–465.

Torres-Ruiz JM, Cochard H, Mayr S, Beikircher B, Diaz-Espejo A, Rodriguez-Dominguez CM, Badel E, Fernández JE. 2014. Vulnerability to cavitation in *Olea europaea* current-year shoots: further evidence of an open-vessel artifact associated with centrifuge and air-injection techniques. *Physiologia Plantarum* **152**: 465–474.

Torres-Ruiz JM, Jansen S, Choat B, McElrone AJ, Cochard H, Brodribb TJ, Badel E, Burlett R, Bouche PS, Brodersen CR *et al*. 2015. Direct X-Ray Microtomography Observation Confirms the Induction of Embolism upon Xylem Cutting under Tension. *Plant Physiology* **167**: 40–43.

Trenberth KE, Dai A, van der Schrier G, Jones PD, Barichivich J, Briffa KR, Sheffield J. 2014. Global warming and changes in drought. *Nature Climate Change* **4**: 17–22.

Trueba S, Pouteau R, Lens F, Feild TS, Isnard S, Olson ME, Delzon S. 2017. Vulnerability to xylem embolism as a major correlate of the environmental distribution of rain forest species on a tropical island. *Plant, Cell & Environment* **40**: 277–289.

Urli M, Porte AJ, Cochard H, Guengant Y, Burlett R, Delzon S. 2013. Xylem embolism threshold for catastrophic hydraulic failure in angiosperm trees. *Tree Physiology* **33**: 672–683.

Venturas MD, Pratt RB, Jacobsen AL, Castro V, Fickle JC, Hacke UG. 2019. Direct comparison of four methods to construct xylem vulnerability curves: Differences among techniques are linked to vessel network characteristics. *Plant, Cell & Environment* **42**: 2422–2436.

Wheeler JK, Huggett BA, Tofte AN, Rockwell FE, Holbrook NM. 2013. Cutting xylem under tension or supersaturated with gas can generate PLC and the appearance of rapid recovery from embolism: Sampling induced embolism. *Plant, Cell & Environment* **36**: 1938–1949.

Wheeler JK, Sperry JS, Hacke UG, Hoang N. 2005. Inter-vessel pitting and cavitation in woody Rosaceae and other vesselled plants: a basis for a safety versus efficiency trade-off in xylem transport. *Plant, Cell & Environment* **28**: 800–812.

Wickham H, Averick M, Bryan J, Chang W, McGowan LD, François R, Grolemund G, Hayes A, Henry L, Hester J, *et al*. 2019. Welcome to the Tidyverse. *Journal of Open Source Software* **4**: 1686.

Wolfe BT, Sperry JS, Kursar TA. 2016. Does leaf shedding protect stems from cavitation during seasonal droughts? A test of the hydraulic fuse hypothesis. *New Phytologist* **212**: 1007–1018.

Wu M, Zhang Y, Oya T, Marcati CR, Pereira L, Jansen S. 2020. Root xylem in three woody angiosperm species is not more vulnerable to embolism than stem xylem. *Plant and Soil* 450: 479–495.

Xu X, Medvigy D, Powers JS, Becknell JM, Guan K. 2016. Diversity in plant hydraulic traits explains seasonal and inter-annual variations of vegetation dynamics in seasonally dry tropical forests. *New Phytologist* **212**: 80–95.

Yang D., Pereira P., Peng G., Ribeiro R.V., Kaack L., Jansen S., Tyree M.T. Submitted. A Unit Pipe Pneumatic model to simulate gas kinetics during measurements of embolism in excised angiosperm xylem. bioRxiv, https://doi.org/10.1101/2021.02.09.430450.

Zhang Y, Lamarque LJ, Torres-Ruiz JM, Schuldt B, Karimi Z, Li S, Qin D-W, Bittencourt P, Burlett R, Cao K-F, *et al*. 2018. Testing the plant pneumatic method to estimate xylem embolism resistance in stems of temperate trees. *Tree Physiology* **38**: 1016–1025.

Zhao H, Jiang Z, Ma J, Cai J. 2020. What causes the differences in cavitation resistance of two shrubs? Wood anatomical explanations and reliability testing of vulnerability curves. *Physiologia Plantarum* **169**: 156–168.

749 **Zhu S-D, Liu H, Xu Q-Y, Cao K-F, Ye Q. 2016.** Are leaves more vulnerable to cavitation than
750 branches? *Functional Ecology* **30**: 1740–1744.

751 **Zimmermann U, Wagner H-J, Heidecker M, Mimietz S, Schneider H, Szimtenings M, Haase A,**
752 **Mitlöhner R, Kruck W, Hoffmann R, *et al*. 2002.** Implications of mucilage on pressure bomb
753 measurements and water lifting in trees rooting in high-salinity water. *Trees* **16**: 100–111.

Tables

Table 1: List of the 12 diffuse-porous tree species used in the present study, average midday leaf water potential (Ψ_{midday}) measured in August 2020 and the average diameter at breast height (DBH) of the selected trees per species (mean ± SE); n_P and n_H indicate the number of xylem vulnerability curves measured for the pneumatic and the flow-centrifuge method, respectively (values in brackets indicate when branch samples were collected from a single tree). Asterisks (*) indicate xylem pressures measured with stem psychrometers; hashes (#) indicate individuals from the same species measured with the pressure bomb.

Species	Family	n_P	n_H	Ψ_{midday} (MPa)	DBH (cm)
Betula pendula	Betulaceae	3	3	-1.60 ± 0.04	10.93 ± 0.64
Betula utilis	Betulaceae	3	3	-1.54 ± 0.06	08.88 ± 0.42
Carpinus betulus	Betulaceae	3	3	-2.47 ± 0.06	10.75 ± 0.44
Crataegus persimilis	Rosaceae	3	3	-3.42 ± 0.18	07.55 ± 0.16
Ostrya carpinifolia	Betulaceae	3	3	-2.97 ± 0.11	09.18 ± 0.11
Platanus x acerifolia	Platanaceae	3	3	-1.74 ± 0.03	10.00 ± 0.24
Platanus orientalis	Platanaceae	3	3	-1.51 ± 0.04	12.07 ± 0.35
Pyrus calleryana	Rosaceae	2	3	-3.52 ± 0.30	11.88 ± 0.32
Sorbus latifolia	Rosaceae	3	3	-3.64 ± 0.19	09.30 ± 0.39
*Tilia cordata**	Malvaceae	5(1)	5(1)	NA	28.00 ± 0.00
Tilia cordata#	Malvaceae	3	3	-1.90 ± 0.04	11.40 ± 0.46
Tilia japonica	Malvaceae	3(1)	4(1)	NA	30.40 ± 0.00
*Tilia platyphyllos**	Malvaceae	4(1)	7(1)	NA	70.00 ± 0.21
Tilia platyphyllos#	Malvaceae	3	3	-1.80 ± 0.08	12.38 ± 0.21

Table 2: Parameter estimates of the linear mixed effect models for the xylem water potential at 12%, 50% and 88% loss of conductivity (P_{12}, P_{50} and P_{88}, respectively) and the natural log-transformed slope at 50% loss of conductivity (S_{50}). Given are estimates for the intercept (average for flow-centrifuge based reference value) as well as the differences from the reference for different AD times, with the corresponding standard errors, *t*-statistics, approximate degrees of freedom based on the Satterthwaite approximation and corresponding *P*-values.

Parameter	Treatment	Estimate	Std.error	*t*-statistic	edf	*P*-value
P_{12}	(Intercept)	-2.814	0.32	-8.79	12.085	< 0.001
	Δ 15 s	0.444	0.086	5.144	198.53	< 0.001
	Δ 30 s	0.532	0.086	6.163	198.53	< 0.001
	Δ 60 s	0.631	0.086	7.311	198.53	< 0.001
	Δ 90 s	0.702	0.086	8.13	198.53	< 0.001
	Δ 115 s	0.758	0.086	8.781	198.53	< 0.001
P_{50}	(Intercept)	-3.652	0.495	-7.383	11.154	< 0.001
	Δ 15 s	0.114	0.056	2.037	202.67	0.043
	Δ 30 s	0.184	0.056	3.284	202.67	0.001
	Δ 60 s	0.259	0.056	4.632	202.67	< 0.001
	Δ 90 s	0.305	0.056	5.453	202.67	< 0.001
	Δ 115 s	0.332	0.056	5.936	202.67	< 0.001
P_{88}	(Intercept)	-4.512	0.699	-6.451	11.263	< 0.001
	Δ 15 s	-0.213	0.094	-2.265	200.67	0.025
	Δ 30 s	-0.162	0.094	-1.718	200.67	0.087
	Δ 60 s	-0.11	0.094	-1.169	200.67	0.244
	Δ 90 s	-0.089	0.094	-0.945	200.67	0.346
	Δ 115 s	-0.091	0.094	-0.968	200.67	0.334
S_{50}	(Intercept)	4.258	0.2	21.30	12.452	< 0.001
	Δ 15 s	-0.253	0.081	-3.124	204.53	0.002
	Δ 30 s	-0.266	0.081	-3.284	204.53	0.001
	Δ 60 s	-0.287	0.081	-3.536	204.53	< 0.001
	Δ 90 s	-0.303	0.081	-3.742	204.53	< 0.001
	Δ 115 s	-0.326	0.081	-4.022	204.53	< 0.001

Figure captions

Figure 1: Xylem vulnerability curves obtained with the pneumatic method after a measurement duration of 15 sec (green) and the flow-centrifuge method (blue) for 12 diffuse-porous tree species. Circles: observed values (for the centrifuge data, rescaled from conductance to PLC using the estimated k_{sat}); solid lines: predicted PLC/PAD; dashed lines: estimated P_{50}. Asterisks (*) at the end of species names indicate xylem pressure measurements with stem psychrometers.

Figure 2: Relationship between estimates from the flow-centrifuge method (x-axis) and the pneumatic method with 15 sec air discharge interval (y-axis). a) P_{12}, b) P_{50}, c) P_{88} (xylem water potentials at 12%, 50% and 88%, respectively) and d) slope at 50% loss of conductivity (displayed on a log scale). Colours – species identity (empty circles indicate pressure chamber-based *Tilia* measurements); solid black line – standardized major axis (SMA) regression fit through all points ± 95% bootstrap confidence interval; grey dashed line: 1:1 line.

Figure 3: Comparison of P_{50} values between the flow-centrifuge and different air discharge intervals for the pneumatic method (compared on the same branch). C indicates the P_{50} values from the flow-centrifuge method, 15, 30, 60, 90, and 115 indicate AD measurement intervals (in seconds) evaluated from the pneumatic method. Shown are the raw estimates overlaid with their mean ± SE. Asterisks (*) at the end of species name indicate xylem pressure was determined using stem psychrometer.

Figure 4: Statistics describing the agreement between the estimated vulnerability curve parameters from the pneumatic method and the flow-centrifuge method vs. the duration of air

discharge measurement (estimates ± 95% bootstrap confidence intervals based on 1,000 bootstrap draws). The metrics shown are the Pearson correlation (Pearson ρ) as a measure of random deviation between the two methods (values close to one indicate a perfect linear relationship), mean signed deviation (MSD) as a measure of systematic deviations (values close to zero indicate a low bias), and root mean square deviation (RMSD) as a measure of overall agreement (low values indicate a high agreement between methods).

Figure 5: Average L_2 distance between the pneumatic and flow-centrifuge vulnerability curves vs. air discharge time as a measure of overall accuracy (raw averages and ±5 s running average). Vertical lines indicate the minimum of the running average at 16 sec; the shaded area indicates the range with a running average differing from the minimum by less than 1% (10.5 – 44.5 sec).

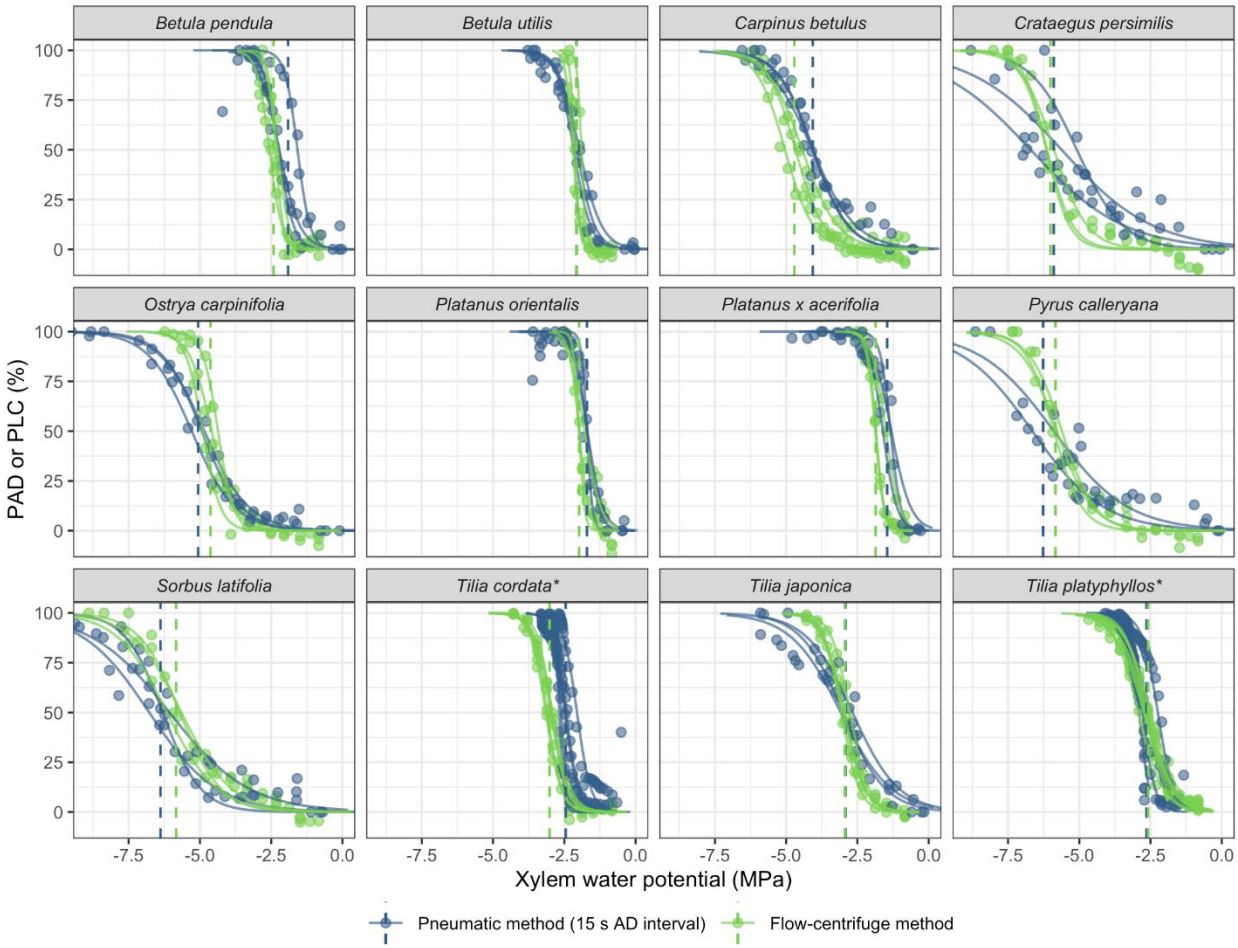

Figure 1

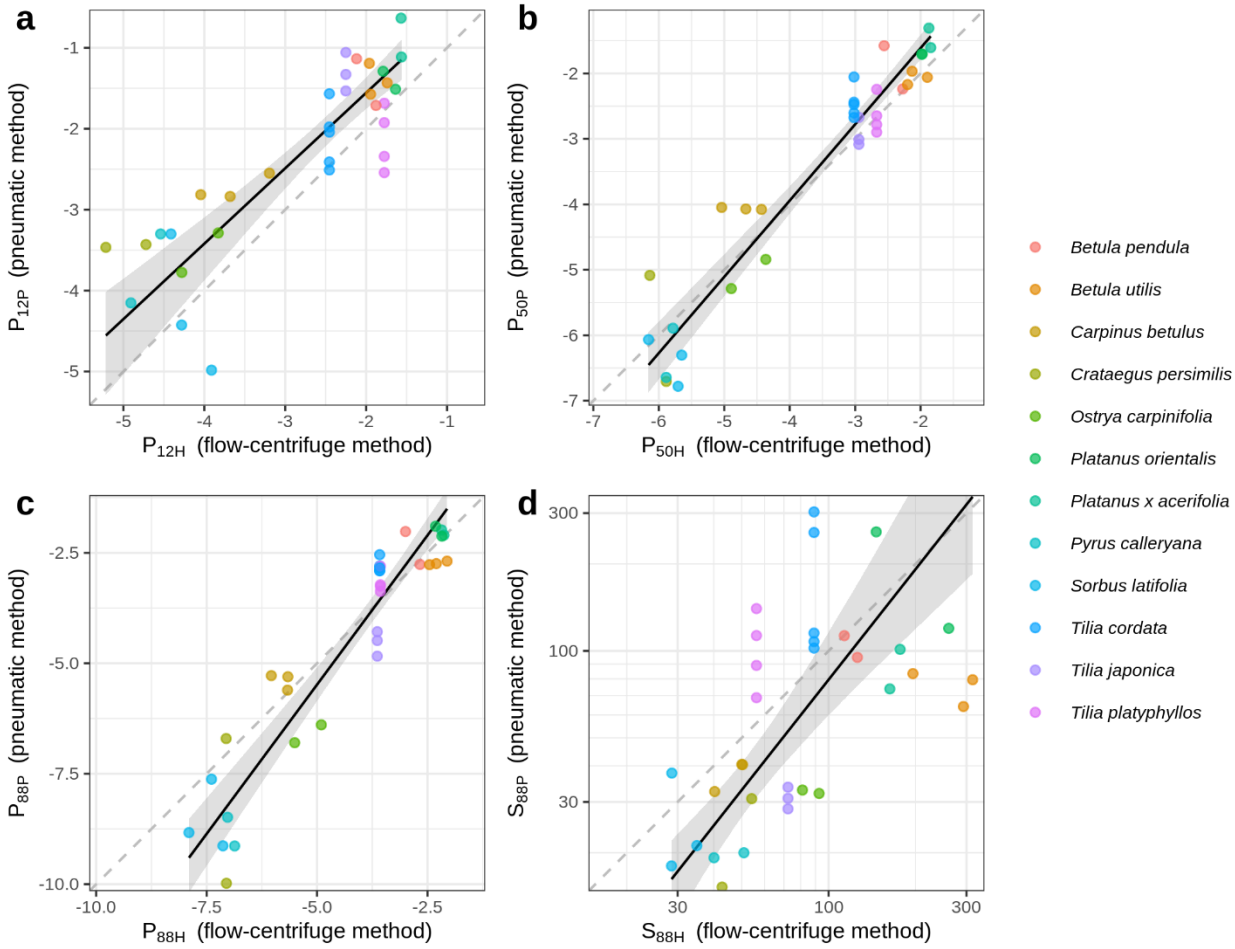

Figure 2

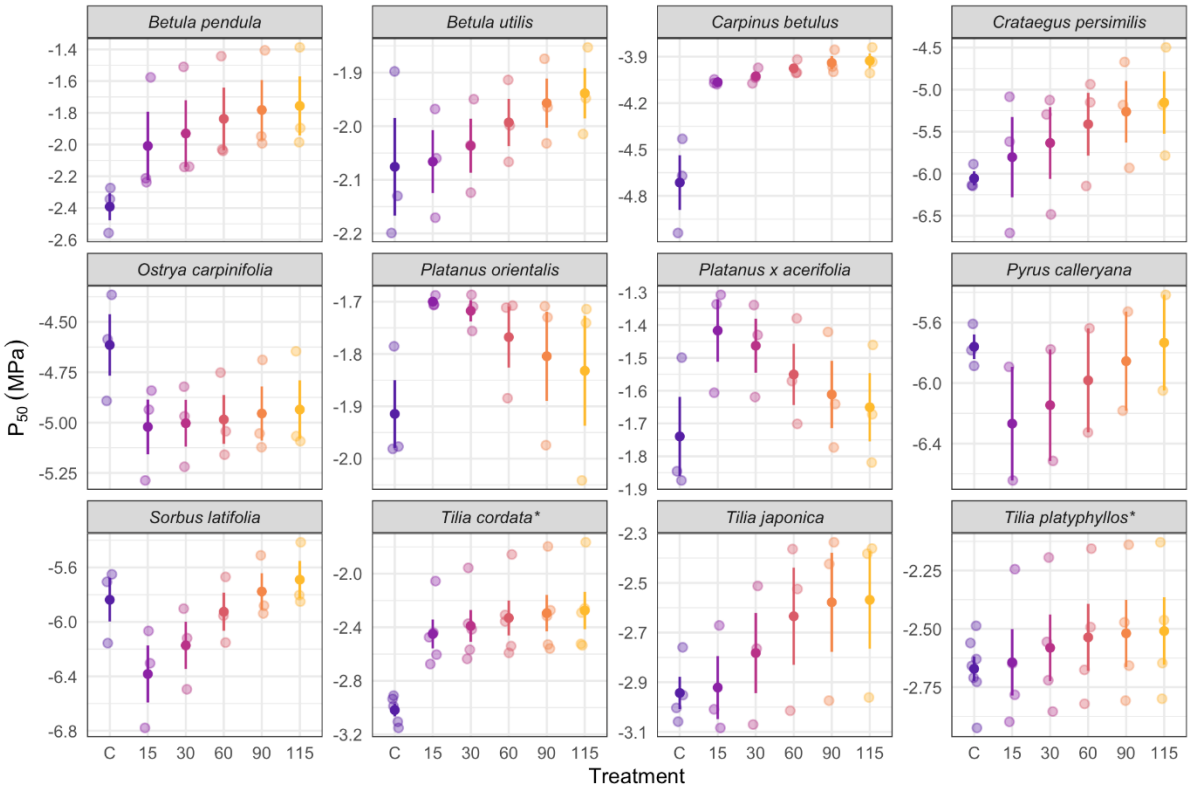

Figure 3

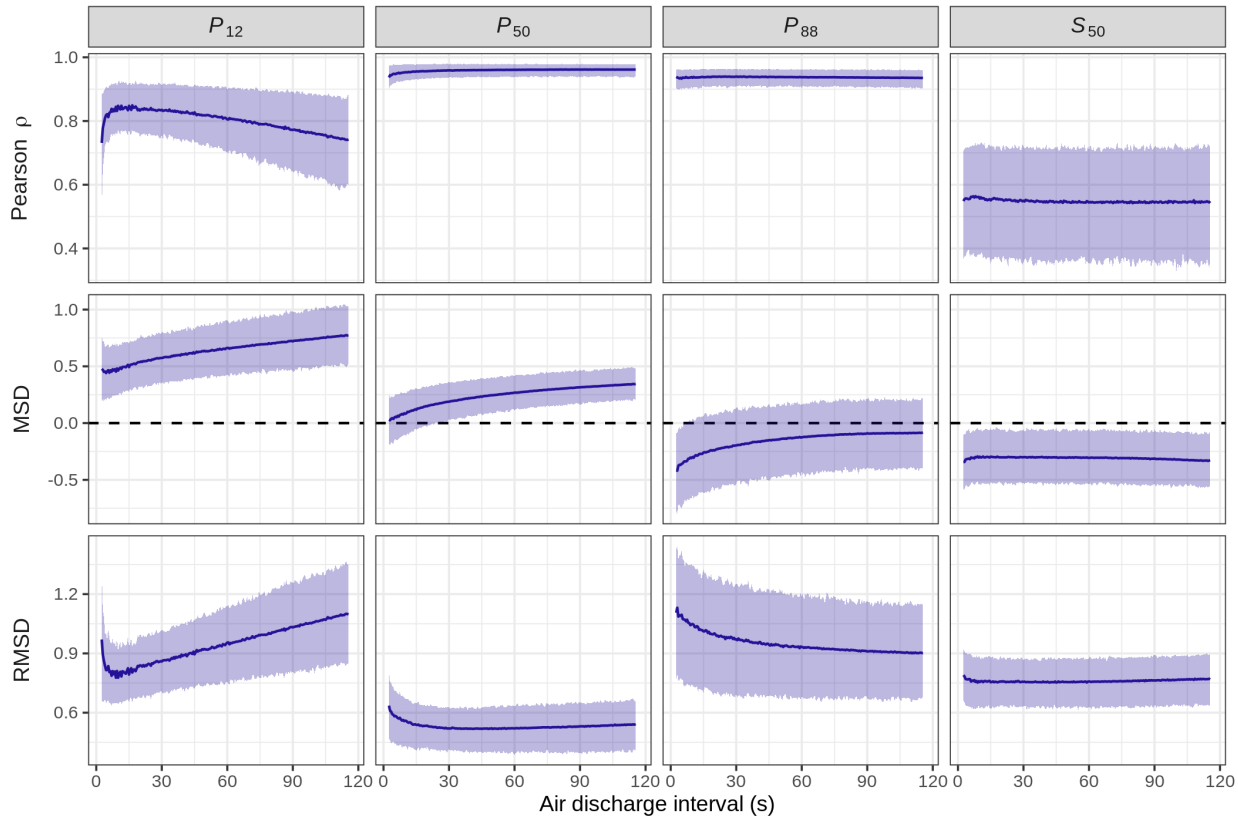

Figure 4

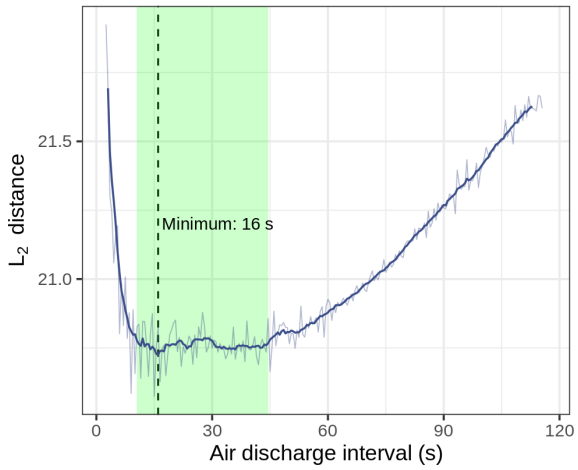

Figure 5